bioRxiv preprint doi: https://doi.org/10.1101/147611; this version posted June 8, 2017. The copyright holder for this preprint (which was not certified by peer review) is the author/funder, who has granted bioRxiv a license to display the preprint in perpetuity. It is made available under aCC-BY-NC-ND 4.0 International license.

NETWORK CONNECTIVITY PREDICTS CORTICAL THINNING AND COGNITIVE DECLINE IN EARLY PARKINSON'S DISEASE

Y. Yau [1], Y. Zeighami [1], T. Baker [2], K. Larcher [1], U. Vainik [1,3], M. Dadar[1], V. Fonov[1], P. Hagmann[4], A. Griffa[5], B. Mišić[1], D.L. Collins[1] & A. Dagher [1]

[1] Montreal Neurological Institute, McGill University, 3801 University Street, Montreal, QC, H3A 2B4, Canada

[2] Center for Molecular and Behavioral Neuroscience, Rutgers University, 197 University Avenue, Newark, NJ, 07102, U.S.A.

[3] Institute of Psychology, Faculty of Social Sciences, University of Tartu, Näituse 2, 50409, Tartu, Estonia

[4] Department of Radiology, Lausanne University Hospital and University of Lausanne, Rue du Bugnon 21, 1011 Lausanne, Switzerland

[5] Brain Center Rudolf Magnus, UMC Utrecht, Heidelberglaan 100, A01.126, 3508 GA Utrecht, Netherlands

bioRxiv preprint doi: https://doi.org/10.1101/147611; this version posted June 8, 2017. The copyright holder for this preprint (which was not certified by peer review) is the author/funder, who has granted bioRxiv a license to display the preprint in perpetuity. It is made available under aCC-BY-NC-ND 4.0 International license.

ABSTRACT

Parkinson's Disease (PD) is a progressive neurodegenerative disorder characterized by motor and cognitive deficits. The neurodegenerative process is thought to move stereotypically from the brainstem up to the cerebral cortex, possibly reflecting the spread of toxic alpha-synuclein molecules. Using a large, longitudinal, multi-center database of *de novo* PD patients, we tested whether focal reductions in cortical thickness could be explained by disease spread from a subcortical "disease reservoir" along the brain's connectome. PD patients (n=105) and matched controls (n=57) underwent T1-MRI at entry and one year later. Over this period, PD patients demonstrated significantly greater loss of cortical thickness than healthy controls in parts of the left occipital and bilateral frontal lobes and right somatomotor-sensory cortex. Cortical regions with greater connectivity (measured functionally or structurally) to a "disease reservoir" evaluated via MRI at baseline demonstrated greater atrophy one year later. The atrophy pattern in the frontal lobes resembled that described in Alzheimer's disease. Moreover, path models suggest that cerebrospinal fluid amyloid-β_{42} predicted left frontal cortical thinning, which in turn was associated with reduced cognitive scores. Our findings suggest that disease propagation to the cortex follows neural connectivity, and that cognitive impairments occur earlier than previously thought in PD.

bioRxiv preprint doi: https://doi.org/10.1101/147611; this version posted June 8, 2017. The copyright holder for this preprint (which was not certified by peer review) is the author/funder, who has granted bioRxiv a license to display the preprint in perpetuity. It is made available under aCC-BY-NC-ND 4.0 International license.

INTRODUCTION

The network spread hypothesis proposes that neurodegenerative diseases target intrinsic brain networks. Specifically, it is suggested that the progression of disease follows network connectivity, and that neurotoxicity is caused by the spread and accumulation of toxic agents along the brain's neuronal connectome[1,2]. In the case of Parkinson's Disease (PD), the agent is thought to be misfolded α-synuclein (α-syn). In its normal conformation, α-syn is an endogenous protein that is soluble and contributes to synaptic vesicular function[3]; however, in synucleinopathies such as PD, α-syn is present in a hyperphosphorylated and insoluble state, and found to adopt an abnormal configuration into amyloid fibril aggregates[4,5]. A model first proposed by Braak suggested patterns of abnormal α-syn accumulation consistent with a stereotyped propagation from brainstem to subcortical areas to cortex, which paralleled the clinical progression of the disease[6]. Numerous lines of evidence support this model: misfolded α-syn aggregates are identified at postmortem in the brains of PD patients, and the protein has been shown to spread through neuroanatomical pathways causing cell death in animal models due to its neurotoxicity[4,5].

There is currently no imaging technique that allows *in vivo* measurement of α-syn level or distribution in the brain. However, we previously observed a pattern of brain atrophy in cross sectional MRI scans of *de novo* PD patients from the Parkinson's Progression Markers Initiative (PPMI) database[7] that was consistent with the network spread hypothesis[8]. The regional distribution of atrophy identified using deformation based morphometry (DBM) targeted an intrinsic connectivity network, and the pattern suggested a disease epicenter in the substantia nigra. The atrophy distribution was mostly subcortical, involving brainstem, striatum, thalamus

bioRxiv preprint doi: https://doi.org/10.1101/147611; this version posted June 8, 2017. The copyright holder for this preprint (which was not certified by peer review) is the author/funder, who has granted bioRxiv a license to display the preprint in perpetuity. It is made available under aCC-BY-NC-ND 4.0 International license.

and medial temporal lobe. Here we make use of the longitudinal data collected at diagnosis and one-year later from the PPMI cohort to test the hypothesis that disease spread from this initial subcortical "disease reservoir" to cortical regions is best explained by propagation via the brain's intrinsic connectome.

Furthermore, disease spread to cortical areas may be accompanied by the start of cognitive impairment. Dementia is now recognized as a common, perhaps inevitable, feature of PD[9,10]. Cognitive impairment takes several forms, starting with executive (frontal lobe) dysfunction and apathy, and progressing to visual hallucinations, impulse control and behavioral disorders, and, eventually, a global cognitive impairment that resembles Alzheimer's Disease (AD)[10-13]. As with the classical dementias, it is likely that the specific pattern of disease spread in PD may shape the clinical features of the dementing process[1].

Recent studies using voxel based morphometry (VBM) to assess grey matter density have begun to highlight a pattern of cortical changes in PD[14,15], but there have been discrepant findings[16,17]**.** Inconsistencies are in-part due to heterogeneity in disease progression and small sample sizes, but also to methodological issues[18]. Cortical thickness analysis may be better able to delineate cortical morphometrical patterns and may be more sensitive to age or disease-related regional grey matter changes than VBM[19,20]. While cortical thinning is normal in the aging process[21], deviations from typical patterns can be used as diagnostic indicators for neurodegenerative disorders (e.g., Alzheimer's disease) even at early stages[22]. Several cross-sectional studies of MRI-derived cortical thickness in early stage PD have reported cortical thinning in parietal and premotor regions compared to controls[20,23-25]. Moreover, cortical thinning appears to correlate

bioRxiv preprint doi: https://doi.org/10.1101/147611; this version posted June 8, 2017. The copyright holder for this preprint (which was not certified by peer review) is the author/funder, who has granted bioRxiv a license to display the preprint in perpetuity. It is made available under aCC-BY-NC-ND 4.0 International license.

with poorer cognitive performance[26]. However, cortical thickness in PD has yet to be studied in a longitudinal setting and little is known how it may correlate with other disease-related measures.

Here we take advantage of follow-up imaging in a large longitudinal, multi-center study that aimed to assess the progression of clinical features, imaging, and other biomarkers in a cohort of well-characterized *de novo* PD patients. Using the PPMI database (http://www.ppmi-info.org/data), we test the theory that disease progression at a one-year follow-up, as assessed by cortical thickness, is best explained by spread from a "disease reservoir" along the brain's connectome. We further ask what factors at baseline predict severity of disease progression at follow-up, and whether cortical involvement might herald the onset of dementia.

RESULTS

Participants in the present study consisted of *de novo* PD patients (n=105) and healthy controls (HC, n=57) enrolled in the PPMI study[7] [accessed May 01, 2016] who had follow-up assessment one-year post-enrollment. Demographic and clinical data are summarized in Table 1. PD patients were unmedicated at the first evaluation. At one-year follow-up, 81 of 105 were on PD medication (e.g., levodopa or dopamine agonist). Among PD patients, performance on the Montreal Cognitive Assessment (MoCA) was slightly worse at follow-up compared to baseline (from 27.5 to 26.7, $t(103)=3.038$, $p=.003$). PD patients also scored higher on the Movement Disorders Society Unified Parkinson's Disease Rating Scale Part III (UPDRS-III) at follow-up compared to baseline, but this did not reach statistical significance (from 21.7 to 23.1, $t(95)=-1.544$, $p=.126$).

bioRxiv preprint doi: https://doi.org/10.1101/147611; this version posted June 8, 2017. The copyright holder for this preprint (which was not certified by peer review) is the author/funder, who has granted bioRxiv a license to display the preprint in perpetuity. It is made available under aCC-BY-NC-ND 4.0 International license.

Table 1. *Demographics, and clinical and neuropsychological measures. t_1: measures at entry. t_2: measures at one-year follow-up.*

	PD patients	**Healthy Controls**	***t*-test/χ^2**	***p*-value**
Age				
t_1	61.06 ±9.37	59.05 ±10.96	1.224	.223
t_2	62.11 ±9.37	60.10 ±10.96	1.223	.223
Sex	33F:72M	22F:35M	0.846	.358
UPDRS-III				
t_1	21.67 ±9.61	----	----	----
t_2	23.10 ±10.67	----	----	----
MoCA				
t_1	27.49 ±2.11	28.30 ±1.13	-3.162	.002*
t_2	26.67 ±2.78	27.35 ±2.01	-1.778	.077
α-syn t_1	1841.54 ±729.73	1898.84 ±753.12	-0.462	.645
Aβ42 t_1	370.33 ±97.02	373.36 ±92.53	-0.189	.850
t-tau t_1	44.77 ±18.36	46.06 ±19.69	-0.407	.684
p-tau181 t_1	15.85 ±9.74	17.30 ±9.84	-0.885	.377

values are expressed as mean ± standard deviation; * = p<.01; t_1 = baseline; t_2 = one-year follow-up

bioRxiv preprint doi: https://doi.org/10.1101/147611; this version posted June 8, 2017. The copyright holder for this preprint (which was not certified by peer review) is the author/funder, who has granted bioRxiv a license to display the preprint in perpetuity. It is made available under aCC-BY-NC-ND 4.0 International license.

Changes in Cortical Thickness at One-Year Follow-Up

Over the one-year period, mean whole-brain cortical thickness significantly decreased amongst both PD patients (t_1 = 3.055mm±0.013; t_2 = 3.027mm±0.013) and controls (t_1 = 3.055mm±0.016; t_2 = 3.036mm±0.017) (both p<0.01). Regional cortical thinning was greater in PD than HC (Figure 1).

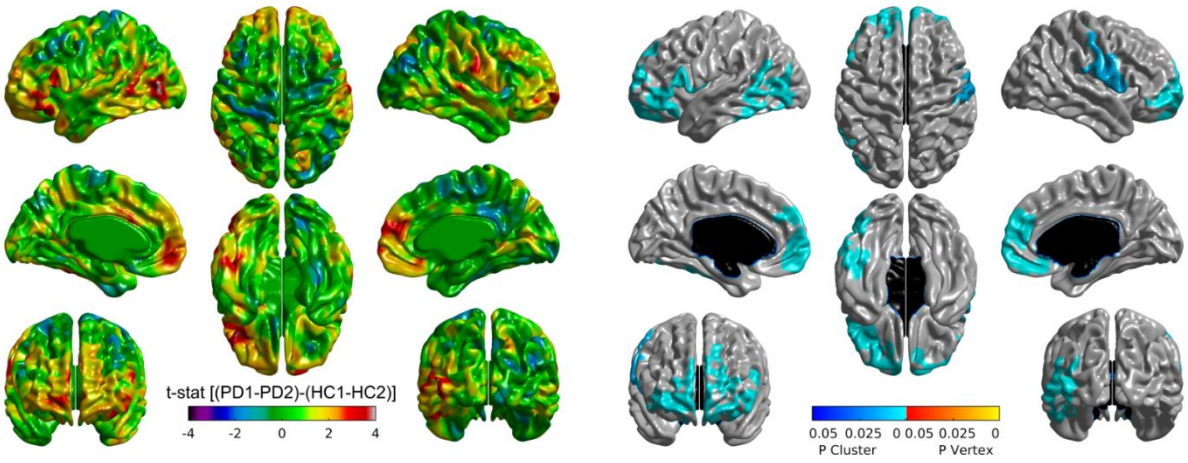

Figure 1. *Changes in cortical thickness in PD patients compared to healthy controls over the one-year study period. Left panel: t-statistic comparing PD to HC at baseline and follow-up, at each cortical vertex. Right panel: thresholded map showing areas of significant difference. Cluster corrected p-value in blue.*

Specifically, four significant clusters were identified: left occipital and inferior and middle temporal gyri, left frontal, right frontal, and right pre- and post-central gyrus and supramarginal gyrus (Figure 2). The frontal lobe atrophy mostly involved the inferior parts of lateral and medial frontal cortex, including the orbitofrontal cortex, frontal pole, ventromedial and rostral dorsomedial prefrontal cortex. On the lateral surface inferior and medial frontal gyri were implicated, with extension to the superior frontal gyrus on the left.

bioRxiv preprint doi: https://doi.org/10.1101/147611; this version posted June 8, 2017. The copyright holder for this preprint (which was not certified by peer review) is the author/funder, who has granted bioRxiv a license to display the preprint in perpetuity. It is made available under aCC-BY-NC-ND 4.0 International license.

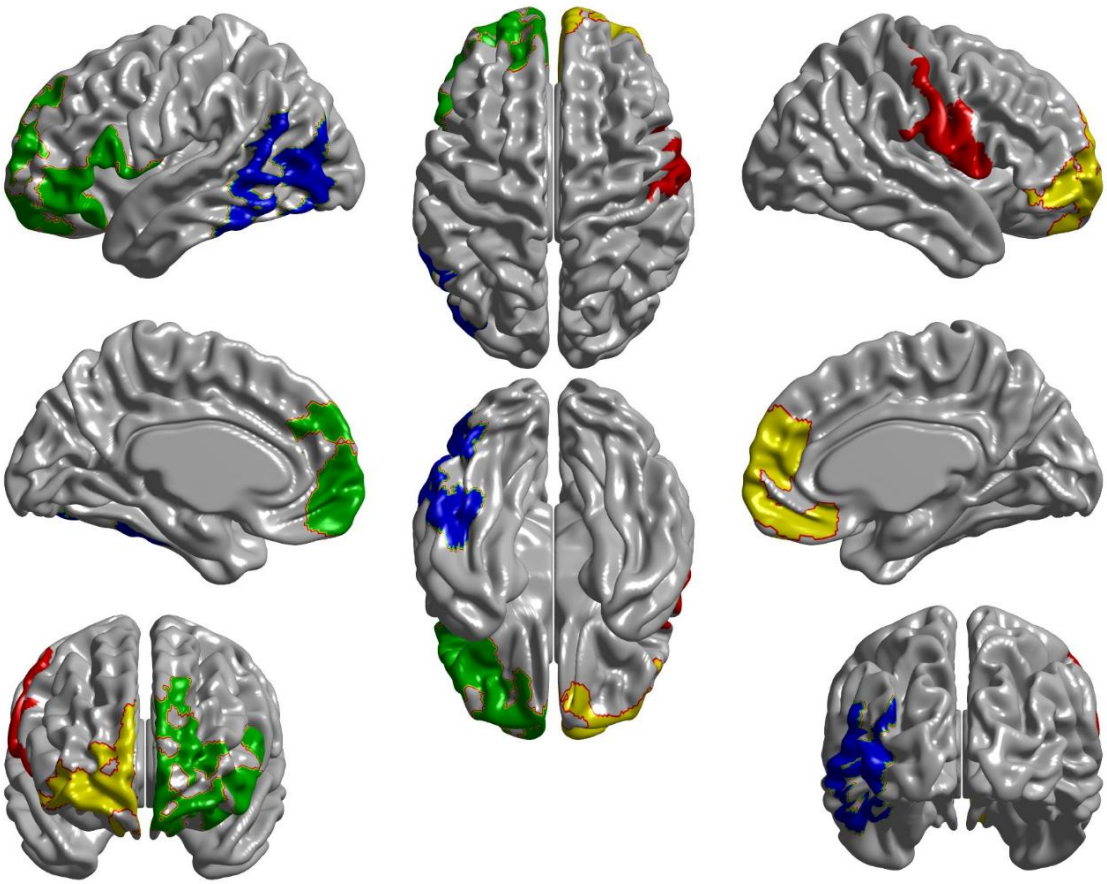

Figure 2. *Differences in cortical thickness between PD and HC over one-year. Four peak clusters of cortical thinning in PD were identified in parts of (1) left occipital lobe (nverts=1081 [5.53 resels], p<.0001, (2) left frontal lobe (nverts=2115 [10.99 resels], p<.0001), (3) right frontal lobe (nverts=3720 [15.79 resels], p<.0001), and (4) right somatomotor cortex (nverts=1990 [16.56 resels], p<.0001). nverts: number of vertices in the significant area.*

bioRxiv preprint doi: https://doi.org/10.1101/147611; this version posted June 8, 2017. The copyright holder for this preprint (which was not certified by peer review) is the author/funder, who has granted bioRxiv a license to display the preprint in perpetuity. It is made available under aCC-BY-NC-ND 4.0 International license.

In the context of the seven intrinsic brain networks derived from resting state fMRI by Yeo, et al.[27], cortical regions belonging to the limbic, frontoparietal, and ventral attention networks on average demonstrated the greatest cortical thinning respectively, as well as anterior parts of the default mode network (Figure 3). There were no areas showing greater loss of cortical thickness in HC than PD.

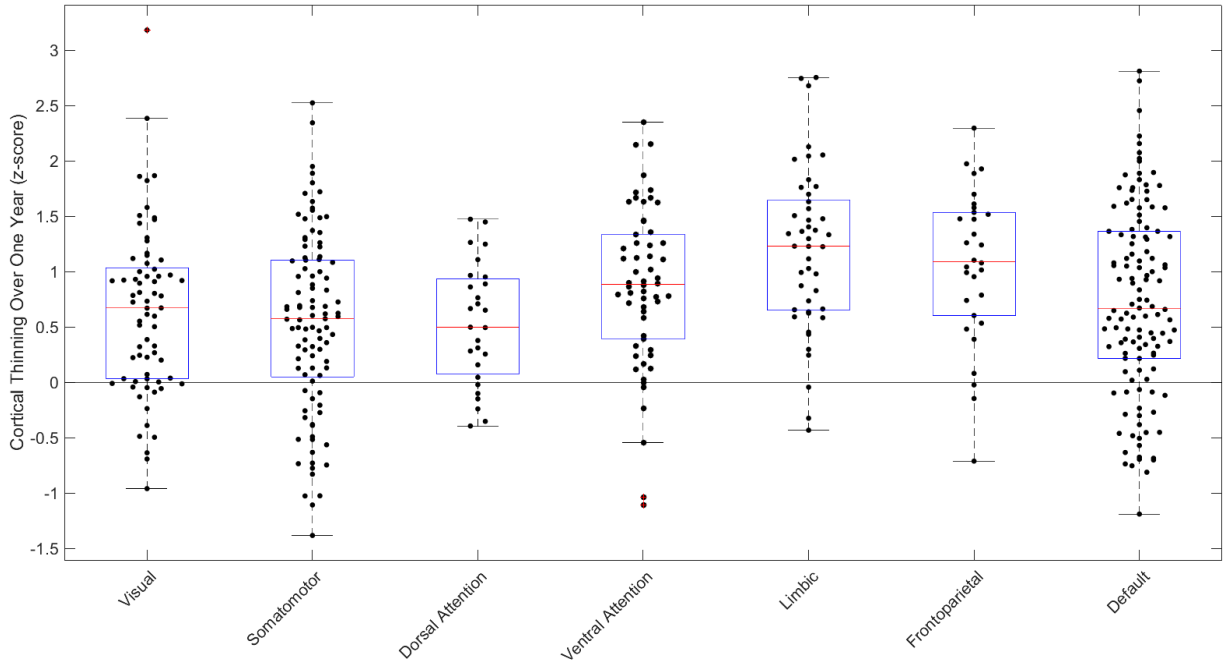

Figure 3. Cortical thinning in PD vs HC in the seven intrinsic brain networks of Yeo et al[27]. *All seven intrinsic brain networks demonstrated significant cortical thinning with ($p<.0001$ permutation test n=10,000): Visual network ($\mu = 0.63; 95\%\ CI \in [0.46,0.81]$), Somamotor network ($\mu = 0.53; 95\%\ CI \in [0.37,0.69]$), Dorsal Attention network ($\mu = 0.52; 95\%\ CI \in [0.32,0.73]$), Ventral Attention network ($\mu = 0.86; 95\%\ CI \in [0.67,1.94]$), Limbic network ($\mu = 1.2; 95\%\ CI \in [0.98,1.40]$), Frontoparietal network ($\mu = 1.05; 95\%\ CI \in [0.80,1.28]$), and Default Mode network ($\mu = 0.73; 95\%\ CI \in [0.57,0.88]$). + outliers within each network.*

bioRxiv preprint doi: https://doi.org/10.1101/147611; this version posted June 8, 2017. The copyright holder for this preprint (which was not certified by peer review) is the author/funder, who has granted bioRxiv a license to display the preprint in perpetuity. It is made available under aCC-BY-NC-ND 4.0 International license.

Additional analyses restricted to the PD group were then performed to investigate the relationship between cortical thinning of the four identified clusters and other disease-related measures. We found that thinning in the left frontal cluster in PD compared to HC, but not in the other clusters, was correlated with the reduction in MoCA score ($r=-0.19$, $p<0.03$). A path model was used to investigate the directed dependencies of CSF measures on cortical thickness in the four clusters, which in turn would influence cognitive performance (as assessed by MoCA) (Figure 4). Path models suggested, that $A\beta_{42}$, α-syn, and T-tau influence cortical thickness change in the left occipital ($A\beta_{42}$: $\beta=-0.18$, $p=0.054$; α-syn: $\beta=-0.19$, $p=0.037$; T-tau: $\beta=-0.22$, $p=0.023$) and left frontal clusters ($A\beta_{42}$: $\beta=-0.18$, $p=0.079$). Change in thickness of left frontal cluster in turn might influence change in MOCA scores ($\beta=-0.24$, $p=0.064$). However, these results are suggestive as demonstrated by the modest beta values.

CSF measures did not correlate with individual time-point measures nor changes in MoCA or motor severity as assessed by UPDRS-III (all $p>.05$). No significant correlation was observed between cortical thickness of any of the four clusters and measures of UPDRS-III or p-tau_{181}. In the control group, no significant correlation between cortical thickness and measures of UPDRS-III, MoCA or CSF biomarkers were observed.

bioRxiv preprint doi: https://doi.org/10.1101/147611; this version posted June 8, 2017. The copyright holder for this preprint (which was not certified by peer review) is the author/funder, who has granted bioRxiv a license to display the preprint in perpetuity. It is made available under aCC-BY-NC-ND 4.0 International license.

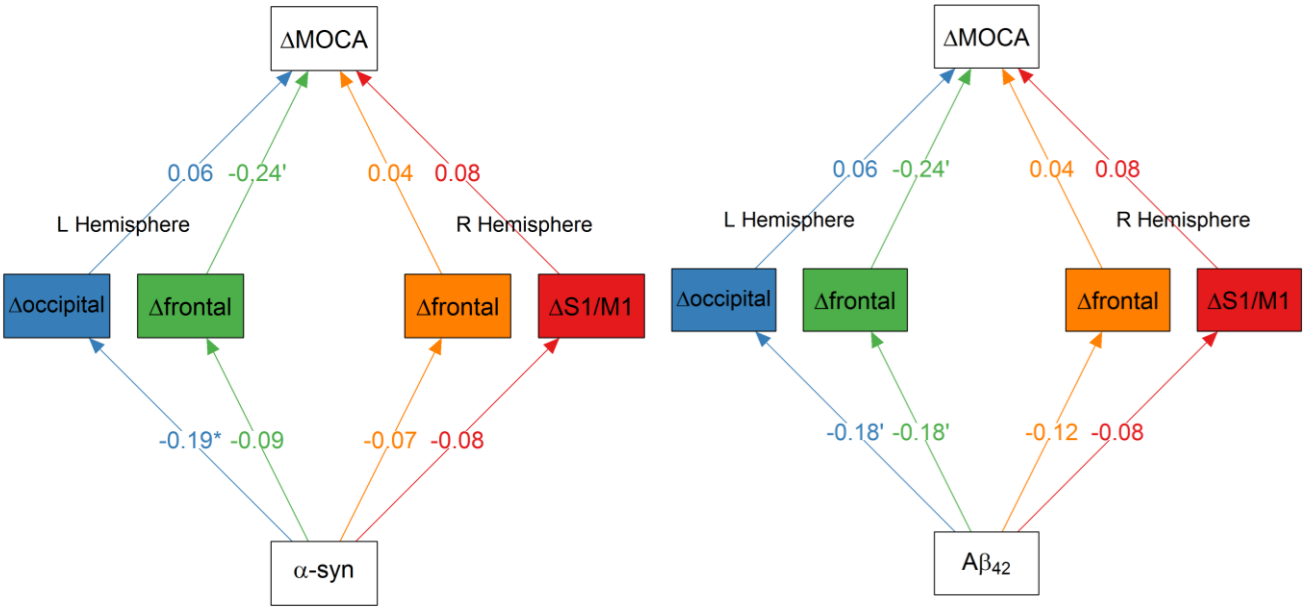

Figure 4. *Path diagrams of CSF measures predicting change (delta) in cortical thickness, and delta cortical thickness predicting change in cognitive score (MOCA). All regressions are standardized and controlled for age and gender. Change in thickness of left hemisphere parcels is partly explained by $A\beta_{42}$ and α-syn, and change in left frontal parcel partly explains variance in change in cognitive performance. * p<0.05; '=p<0.1.*

Connectivity and Disease Propagation

The disease propagation hypothesis predicts that cortical brain atrophy at follow-up should depend on connectivity of cortical areas to affected areas at baseline. We had previously shown predominant subcortical atrophy in *de novo* PD in this population[8]. Connectivity between any cortical area and this putative subcortical "disease reservoir" should therefore predict the degree

bioRxiv preprint doi: https://doi.org/10.1101/147611; this version posted June 8, 2017. The copyright holder for this preprint (which was not certified by peer review) is the author/funder, who has granted bioRxiv a license to display the preprint in perpetuity. It is made available under aCC-BY-NC-ND 4.0 International license.

of cortical thinning relative to age-matched controls when comparing follow-up to baseline. We define the disease reservoir as the areas showing atrophy in PD patients relative to controls at the initial evaluation, as determined previously using DBM[8]. For the current analysis, the brain was segmented into 463 cortical and subcortical regions of interest[28]. Each surface vertex from the cortical thickness images was mapped to the nearest volumetric parcel (see Methods). Then to examine the propagation hypothesis, the connectivity ($Conn_{ij}$) between any cortical parcel *i* and any parcel belonging to the disease reservoir *j* was measured. Here we calculated $Conn_{ij}$ based on normal brain connectomes. The analysis was performed for the whole brain, and for each hemisphere separately. Disease exposure was defined as the product of connectivity and atrophy measure in the corresponding disease reservoir region *j* at the onset of the disease, summed over all possible connections.

$$Disease\ Exposure(i) = \sum_{j} Conn_{ij} \cdot Atrophy(j)$$

Both functional and structural connectivity were used to test the propagation hypothesis (Figure 5). Connectomes were generated using data from young healthy individuals to calculate the $Conn_{ij}$. Atrophy(j) was set equal to the value at each region *j* of the independent component demonstrating atrophy in PD compared to HC from the previously computed DBM map from the baseline MRI[8]. Note that for areas not showing significant atrophy at baseline the value of *Atrophy(j)* is equal to 0.

First, a functional connectome was generated using resting state fMRI to define $Conn_{ij}$. Significant correlation was observed between regional cortical thinning and disease exposure ($r=0.18$, $p<0.0002$). Significance was confirmed by permutation testing where we kept the

bioRxiv preprint doi: https://doi.org/10.1101/147611; this version posted June 8, 2017. The copyright holder for this preprint (which was not certified by peer review) is the author/funder, who has granted bioRxiv a license to display the preprint in perpetuity. It is made available under aCC-BY-NC-ND 4.0 International license.

connectivity structure (i.e. subcortical-cortical connections) intact and permuted the cortical thinning values (n=10,000) and the 95% confidence interval was measured using bootstrapping (n=10,000) ($r \in [0.10,0.25]$, p_perm=0.0001). Moreover, cortical thickness of both the left ($r=0.19$, $p<0.003$, r[0.07,0.29], p_perm=0.0025) and right hemisphere ($r=0.21$, $p<0.0002$, $r \in [0.16,0.34]$, p_perm=0.0001) significantly correlated with the disease exposure from bilateral affected regions.

Second, the same hypothesis was tested using structural connectivity as measured by diffusion-weighted MRI (DW-MRI). Though the correlation was not significant at the whole-brain level ($r= -0.02$, p=0.0.32, $r \in [0.12,0.08]$, p_perm=0.65), change in cortical thickness and disease exposure within the individual hemispheres were significantly correlated. Similar results were observed within the left hemisphere ($r=0.2$, $p<0.003$, $r \in [0.07,0.33]$, p_perm=0.0015) and the right hemisphere ($r=0.15$, $p<0.02$, $r \in [0.01,0.30]$, p_perm=0.0095). Failure to capture the relationship at the whole brain level may be due to inherent limitations in DW-MRI to detect interhemispheric connectivity.

bioRxiv preprint doi: https://doi.org/10.1101/147611; this version posted June 8, 2017. The copyright holder for this preprint (which was not certified by peer review) is the author/funder, who has granted bioRxiv a license to display the preprint in perpetuity. It is made available under aCC-BY-NC-ND 4.0 International license.

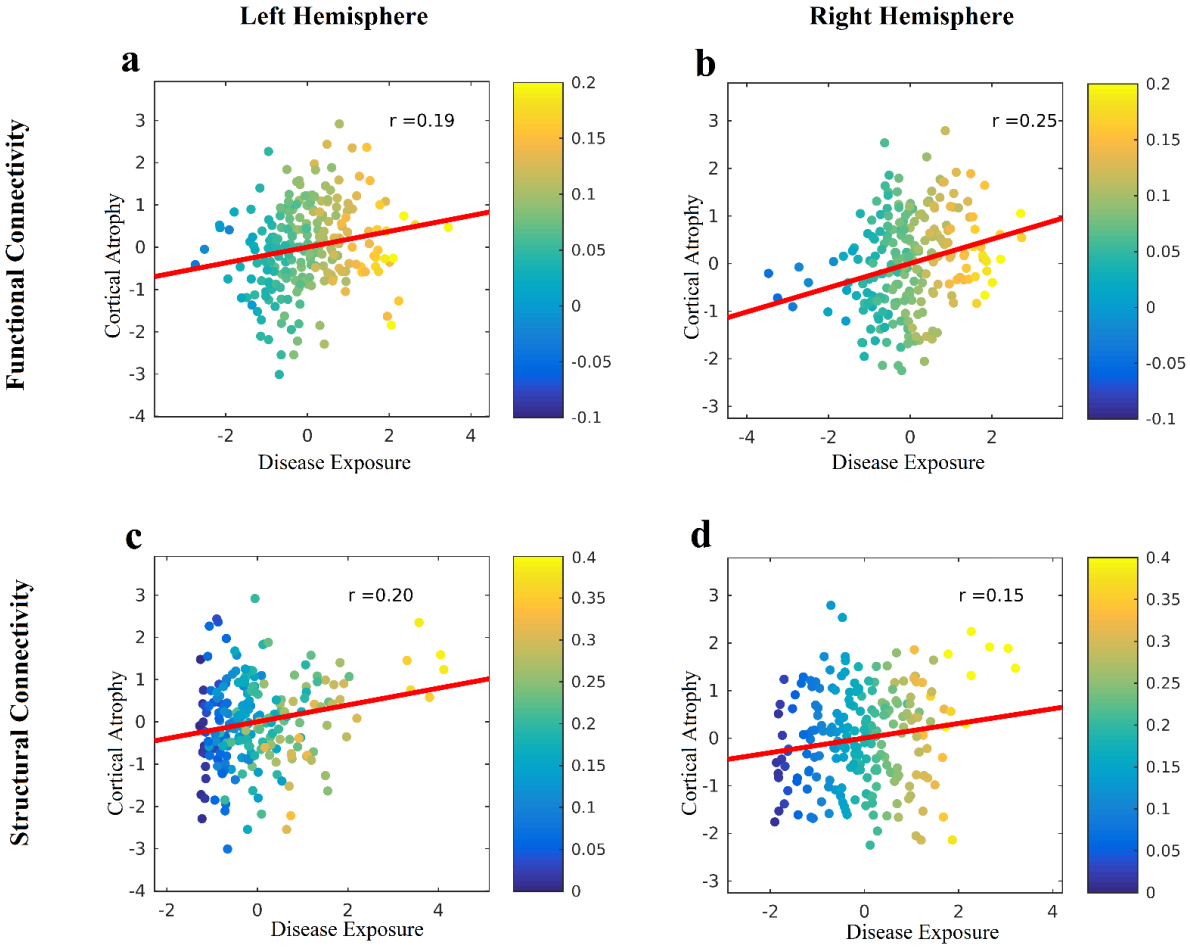

Figure 5. *Correlation between cortical thinning (average t-values, PD-HC, t_2-t_1) of each cortical region and disease exposure (see text for detail). Connectivity based on functional resting state data in the (a) left and (b) right hemisphere as well as connectivity based on structural diffusion-weighted data in the (c) left and (d) right hemisphere are depicted. The color-scale depicts the connectivity strength to subcortical areas irrespective of atrophy.*

bioRxiv preprint doi: https://doi.org/10.1101/147611; this version posted June 8, 2017. The copyright holder for this preprint (which was not certified by peer review) is the author/funder, who has granted bioRxiv a license to display the preprint in perpetuity. It is made available under aCC-BY-NC-ND 4.0 International license.

DISCUSSION

The present study investigated 105 PD and 57 control participants over a one-year period following initial diagnosis. Early PD progression was associated with significant cortical changes. While aging was also associated with cortical thinning, PD patients demonstrated significantly greater reduction in cortical thickness than controls (0.028mm vs 0.019mm reduction on average). This was observed mostly in parts of the left occipital and bilateral frontal lobes and right somatomotor-sensory cortex – regions largely belonging to the limbic, frontoparietal, ventral attention and default mode networks. Within PD, greater reduction in cortical thickness of the left frontal cluster over the one-year period was associated with worsening cognition (as assessed by the MoCA). Cortical neuronal degeneration could be occurring earlier in the clinical course of PD than once thought. Although PD is primarily thought of as a movement disorder, it is recognized to be a brain-wide neurodegenerative process that spreads up from brainstem into cortex, as originally suggested by Braak[29]. Indeed, dementia in PD has a point prevalence of roughly 30% and incidence rates four to six times higher than controls[30]. Our results suggest that even in a dementia-free cohort of *de novo* PD patients, cortical atrophy and cognitive impairment may begin within one to two years of diagnosis.

Baseline CSF $A\beta_{42}$ predicted the loss of cortical thickness in the frontal clusters. The path model (Figure 5) suggests that, among CSF measures, only reduced $A\beta_{42}$ predicted left frontal cortical thinning, which was in turn associated with reduced MoCA score. Lower CSF α-syn was associated only with occipital thinning, which did not correlate with cognitive decline. The frontal clusters demonstrating greater loss of cortical thickness in PD involved lateral and medial frontal cortex, predominantly in ventral and orbitofrontal areas. These regions of frontal lobe

bioRxiv preprint doi: https://doi.org/10.1101/147611; this version posted June 8, 2017. The copyright holder for this preprint (which was not certified by peer review) is the author/funder, who has granted bioRxiv a license to display the preprint in perpetuity. It is made available under aCC-BY-NC-ND 4.0 International license.

belong to the limbic system, the frontoparietal systems implicated in focused attention, and the default mode network, implicated in memory retrieval. This pattern of frontal atrophy is similar to that described in a subgroup of AD patients identified by hierarchical clustering[31], and in patients with behavioral variant frontotemporal dementia[1]. A notable difference between the pattern of cortical atrophy described here and that commonly seen in AD is the relative absence of more posterior involvement (precuneus, posterior cingulate and parietal lobe) in our PD cohort. The effect seen here is much more anterior, possibly reflecting the propagation of disease via dopamine projections. Nonetheless, the default mode network is also disrupted in AD[32,33], and a target of amyloid plaques[34]. The anterior default mode network may be an avenue through which dementia develops in PD. We note also that, in the Braak model of AD, the initial cortical site of amyloid-β involvement is the ventral frontal cortex[35], and that the observed ventral frontal atrophy pattern in PD shows a high degree of similarity to early $A\beta_{42}$ deposition measured by positron emission tomography in Alzheimer's Disease[36].

While cognitive impairment is a recognized consequence of PD[9], its underlying mechanism is not well understood. Our findings suggest that, in the PD group, higher $A\beta_{42}$ deposition in the brain at baseline (indicated by lower CSF $A\beta_{42}$ levels[37]) predicted greater cortical thinning of the left frontal cluster over the one-year period. $A\beta_{42}$ may make the PD brain more susceptible to cortical thinning and in turn, more prone to cognitive decline. Indeed, recent positron emission tomography studies have revealed that cortical amyloid deposits are associated, in a dose-dependent manner, with increased risk for cognitive decline in PD[38]. Additionally, low CSF $A\beta_{42}$ has previously been associated with risk of subsequent dementia in PD[39]. These findings provide evidence in favor of potentially overlapping mechanisms for dementia in PD and AD. Previous research found that 28% of PD patients have AD pathological features at post-mortem[40]. A

bioRxiv preprint doi: https://doi.org/10.1101/147611; this version posted June 8, 2017. The copyright holder for this preprint (which was not certified by peer review) is the author/funder, who has granted bioRxiv a license to display the preprint in perpetuity. It is made available under aCC-BY-NC-ND 4.0 International license.

possible explanation is that synergy between $A\beta_{42}$ and α-syn deposition promotes cognitive impairment in PD[41]. $A\beta_{42}$ has been found to promote gray matter atrophy in distributed regions of the parietal and frontal lobe in the normal aging brain[42], akin to the atrophy pattern observed in the present study; α-syn may accelerate the neurodegenerative process associated with normal age-related $A\beta_{42}$ deposition, especially in regions connected to the PD disease reservoir.

We propose that neurodegeneration in PD results from a disease spreading process that enters the cerebral cortex via dopaminergic and basal ganglia projections to the frontal lobes. Per the network propagation hypothesis, neurodegenerative diseases result from the aggregation and propagation of misfolded proteins, which in turn results in neuronal death and brain atrophy[2,5]. We postulate that focal cortical thinning is contingent on connectivity to a disease reservoir, by analogy to the spread of epidemics in populations: connectivity determines disease exposure and spread. In the present study, we tested this hypothesis in PD with longitudinal data. We found that cortical regions with greater connectivity (measured functionally or structurally) to the mostly subcortical disease reservoir demonstrated greater cortical atrophy over the one-year period. This is in line with our previous work using DBM[8], which indicated that regions demonstrating the greatest atrophy were those belonging to a connectivity network with an epicenter in substantia nigra - the hypothesized origin of misfolded protein spread to the supratentorial central nervous system in PD. However, we did not observe structural interhemispheric propagation between disease reservoir and cortical areas, perhaps due to inherent limitations in DW-MRI to capture these connections[43,44] Mathematical models of this dynamic spread through brain networks, accounting for factors such as protein accumulation and clearance, have been proposed in recent years for Alzheimer's Disease[45,46]. However, further research is needed to extend these models to PD.

bioRxiv preprint doi: https://doi.org/10.1101/147611; this version posted June 8, 2017. The copyright holder for this preprint (which was not certified by peer review) is the author/funder, who has granted bioRxiv a license to display the preprint in perpetuity. It is made available under aCC-BY-NC-ND 4.0 International license.

The pattern of cortical atrophy in these de novo PD patients may account for the constellation of mood and cognitive deficits that eventually characterize PD dementia. Involvement of the lateral prefrontal cortex and striatum could lead to executive dysfunction. Inferior frontal areas also affected in behavioural variant frontotemporal dementia may be implicated in apathy, compulsive behaviors, changes in personality, and social deficits. Finally, DMN involvement could account for Alzheimer-like memory deficits while degeneration of ventral visual stream areas could explain visual hallucinations. Using the Neurosynth program and database[47] we searched for the terms most often associated in fMRI publications with each anatomical cluster demonstrating atrophy in PD (Figure 6). The left occipital-temporal cluster is associated with (visual) motion, observation, perception and vision. The right somatomotor-sensory cluster is associated with movement. The frontal clusters are associated with expressions related to language, and to the terms theory of mind, self, social, mentalizing, and memory. The atrophic regions observed here sub-serve the cognitive functions that fail in PD dementia.

bioRxiv preprint doi: https://doi.org/10.1101/147611; this version posted June 8, 2017. The copyright holder for this preprint (which was not certified by peer review) is the author/funder, who has granted bioRxiv a license to display the preprint in perpetuity. It is made available under aCC-BY-NC-ND 4.0 International license.

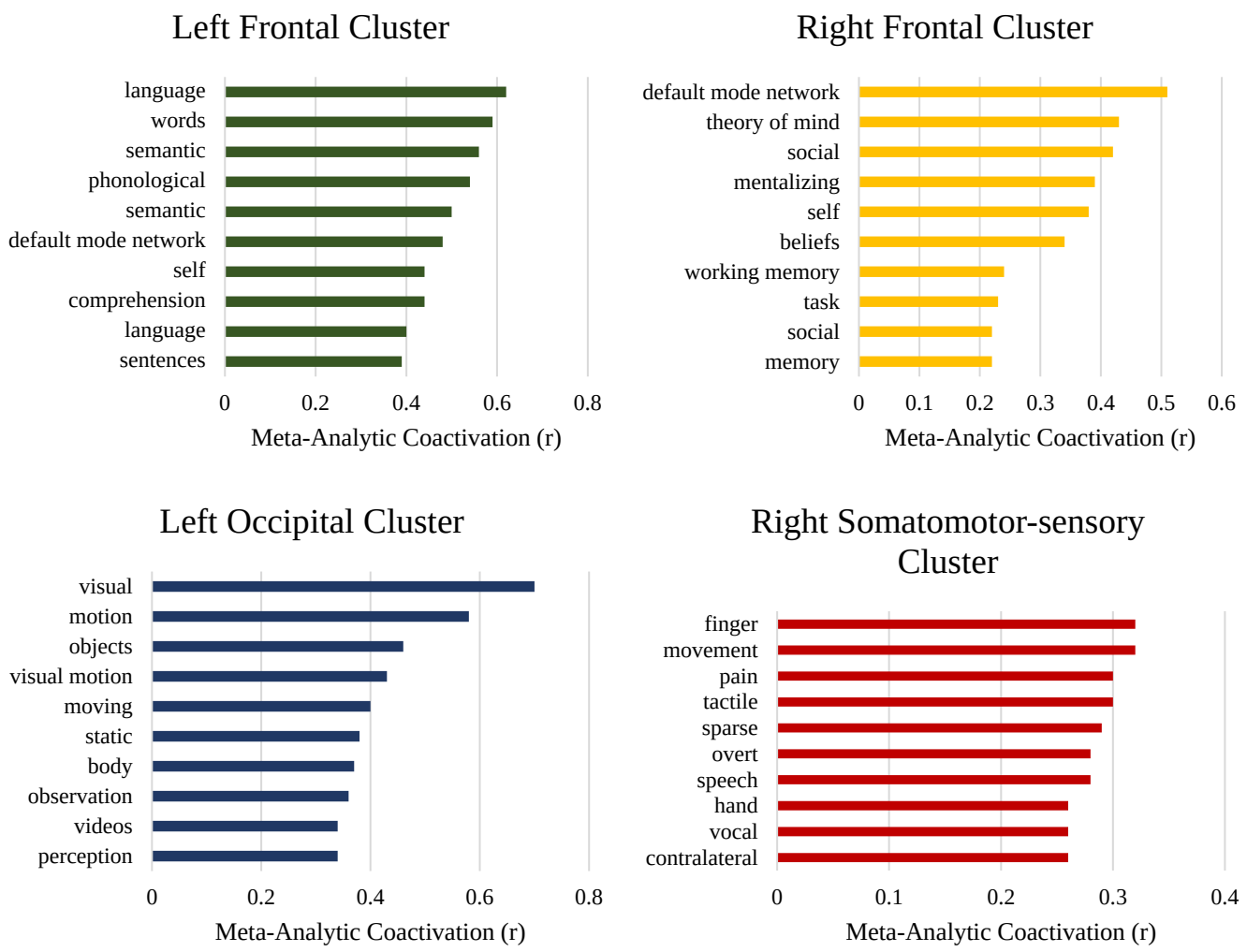

Figure 6. *Peaks within each cluster were associated with expressions used in publications using Neurosynth. The x-axes represent correlation values between the cluster and each concept's meta-analytic map generated using seed-based networks. The y-axes represent the most highly correlated concepts per cluster.*

Findings from this study should be considered in light of some limitations. While the cellular events leading to changes in cortical thickness are not clear, cortical thickness as measured with T1-weighted MRI is nonetheless believed to reflect the neuronal density along with glial support

bioRxiv preprint doi: https://doi.org/10.1101/147611; this version posted June 8, 2017. The copyright holder for this preprint (which was not certified by peer review) is the author/funder, who has granted bioRxiv a license to display the preprint in perpetuity. It is made available under aCC-BY-NC-ND 4.0 International license.

and dendritic arborization[48,49]. In PD, reductions in cortical thickness most likely reflect neurodegeneration. The inclusion criterion of MoCA>26 may have biased both the PD and HC pool. Also, while our sample is relatively large, the PPMI sample is a research-based cohort and may not be truly representative of a population-based cohort. Finally, most patients were prescribed dopaminergic treatments after diagnosis, which may mask the magnitude of cognitive decline and motor symptoms and their relationship with brain atrophy. Future longitudinal studies and follow-up with patients at later stages of the disease as well as postmortem confirmation are needed to understand the relationship between cortical atrophy and the underlying disease process.

The current study is the largest to date to assess longitudinal measures of cortical thickness using 3T MRI in a *de novo* PD cohort. Our findings suggest that disease propagation to the cortex occurs earlier than previously thought. Focal cortical thinning may be contingent on connectivity to a disease reservoir: the greater the connections, the higher the disease exposure, and the more the cortical atrophy. PD progression involves subcortical α-syn spreading through intrinsic brain networks to the cortex, possibly in synergy with $A\beta_{42}$, which may be the harbinger of dementia.

METHODS

Eligibility criteria and study procedures have been previously detailed[7]. Each participating PPMI site received approval from their local institutional review board, and obtained written informed consent from all subjects. Analysis of this dataset was approved by the Montreal Neurological Institute Research Ethics Board. Only participants with 3T MRI data at both initial visit and one-

bioRxiv preprint doi: https://doi.org/10.1101/147611; this version posted June 8, 2017. The copyright holder for this preprint (which was not certified by peer review) is the author/funder, who has granted bioRxiv a license to display the preprint in perpetuity. It is made available under aCC-BY-NC-ND 4.0 International license.

year follow-up were included in the present study. Of the 237 PD patients with 3T acquisition at baseline, 122 had MRI data at the one-year follow-up. For controls, 118 subjects had 3T acquisition at baseline, and 62 had MRI data at the one-year follow-up.

All non-categorical data were normally distributed as per Shapiro-Wilk tests. Group difference in sociodemographic and neuropsychological variables were analyzed using the χ^2 test for categorical data, and *t*-test for normally distributed data.

MRI Acquisition

T1-weighted MRI scans were acquired in the sagittal plane on 3T scanners at each study site using a magnetization-prepared rapid-acquisition gradient echo sequence (full study protocol: http://www.ppmi-info.org/study-design/research-documents-and-sops/). Acquisition parameters were as follows: repetition time = 2,300/1,900ms; echo time = 2.98/2.96/2.27/2.48/2.52ms; inversion time = 900ms; flip angle: 9°; 256 × 256 matrix; and 1 × 1 × 1 mm^5 isotropic voxel. Acquisition site was used as a covariate in all analyses.

Cortical Thickness

Cortical thickness models were generated from the T1-weighted 3T MRI scans using the CIVET2.1 preprocessing pipeline[50]. A summary of the steps involved follows; further details can be found online (http://www.bic.mni.mcgill.ca/ServicesSoftware/CIVET). The T1-weighted MRIs were linearly registered to the MNI -ICBM152 volumetric template[51,52]. Images were then

bioRxiv preprint doi: https://doi.org/10.1101/147611; this version posted June 8, 2017. The copyright holder for this preprint (which was not certified by peer review) is the author/funder, who has granted bioRxiv a license to display the preprint in perpetuity. It is made available under aCC-BY-NC-ND 4.0 International license.

corrected for signal intensity non-uniformity[53], and a brain mask was calculated from each input image. Images were then segmented into grey matter, white matter, CSF, and background[50]. After the CIVET pipeline, quality control was carried out by 2 independent reviewers using previously described criteria[54] to ensure adequate quality of the T1-wieghted volume images, such as linear and nonlinear registration, and to exclude distortions in grey and white matter surfaces, and motion artifacts. 17 of 122 PD and 5 of 62 HC failed quality control.

The distance between corresponding vertices of inner and outer cortical surfaces were evaluated by a fully automated method (Constrained Laplacian Anatomic Segmentation using Proximity algorithm)[55] to provide a measure of cortical thickness at each vertex. The white and grey matter interface was fitted across 40,692 vertices in each hemisphere to create the inner cortical surface, then expanded to fit the grey matter and CSF interface to create the outer cortical surface. The surfaces of each subject were nonlinearly registered to an average surface created from the volumetric ICBM152 template. In order to test the propagation hypothesis, the brain was segmented into 448 cortical and 15 subcortical regions[28], and each of the 40,692 cortical vertices from the cortical thickness analysis was interpolated and assigned to one of the 448 cortical parcels.

Changes in cortical thickness were calculated by subtracting the values ($\Delta t = t_1 - t_2$) at the one year follow-up (t_2) from the baseline (t_1) for both groups using the SurfStat software package (http://www.math.mcgill.ca/keith/surfstat/). Difference between PD and controls [(PD_1-PD_2)-(HC_1-HC_2)] were analyzed statistically based on random field theory with a threshold of $p<.05$[56].

Observed differences in cortical thickness were then correlated to other potential disease-related measures (i.e., UPDRS-III, MoCA, CSF α-syn, and tau and $A\beta_{42}$ markers) using Pearson partial

bioRxiv preprint doi: https://doi.org/10.1101/147611; this version posted June 8, 2017. The copyright holder for this preprint (which was not certified by peer review) is the author/funder, who has granted bioRxiv a license to display the preprint in perpetuity. It is made available under aCC-BY-NC-ND 4.0 International license.

correlations. Within PD patients, the difference in cognitive performance over the one-year interval was examined using path models - these tested the association between CSF measures and changes in cortical thickness, and whether cortical thickness of a specific cluster was in turn linked to cognitive performance. All data was scaled to have mean of 0 and SD of 1 such that regression coefficients were standardized and comparable with correlation statistics. Path models were built with R and lavaan, and visualised with semPlot[57-59]. Age at baseline and sex were used as confounding covariates for all analyses.

Deformation Based Morphometry and Independent Component Analysis

Data were analyzed from the baseline visits of newly diagnosed PD patients (n = 232) and an age-matched control group (n = 117) obtained from the PPMI database. All subjects' initial visit 3T high-resolution T1-weighted MRI scans underwent preprocessing steps including denoising[60], intensity non-uniformity correction[53], and intensity range normalization. Next, each subject's T1-weighted image was first linearly, and then nonlinearly, registered to the MNI-ICBM152 template. Using the resulting non-linear transformation fields, we calculated deformation morphometry maps (i.e. the determinant of the Jacobian matrix of transformation). DBM maps were then concatenated and independent component analysis (ICA) was employed to define independent sources of deformation in the brain. For the resulting ICA components (n=30), the PD group was compared to healthy controls (unpaired t-test). The atrophy level significantly differed between PD and control groups in only one of these components after correcting for multiple comparisons (Bonferroni correction) suggesting this component captures PD-specific alterations in the brain. We used this component (referred to as PD-ICA here) as our atrophy

bioRxiv preprint doi: https://doi.org/10.1101/147611; this version posted June 8, 2017. The copyright holder for this preprint (which was not certified by peer review) is the author/funder, who has granted bioRxiv a license to display the preprint in perpetuity. It is made available under aCC-BY-NC-ND 4.0 International license.

map. The component score (atrophy measure) in PD-ICA for each subject was significantly correlated with disease severity as measured by UPDRS-III and SBR[8].

Connectivity and Disease Propagation

The difference in cortical thinning in PD versus controls was used to define disease progression. DBM on the baseline MRI was employed to assess disease-related brain atrophy and to define a source, or reservoir, for disease propagation. As previously, based on a parcellation that is a subdivision of the common FreeSurfer implementation of the Desikan-Killiany Atlas, grey matter was segmented into 463 regions of interest of approximately similar size. Of these parcels, 448 were cortical and 15 were subcortical (7 in each hemisphere and 1 bilateral brainstem)[28]. Each surface vertex was then mapped to the corresponding whole-brain parcel.

To generate brain networks and connectomes, data-driven brain parcellations from young healthy individuals were used[28]. The functional connectivity map was derived from resting state fMRI data of 40 young healthy subjects (25.3±4.9yr old, 24 males)[61]. The scans were done using Siemens Medical Trio 3T MRI scanner, consisting of a high resolution T1-weighted image, as well as T2*-weighted images with BOLD contrast (3.3 mm isotropic voxels, TR 1.9s). The structural connectivity map was generated using the Illinois Institute of Technology Human Brain Atlas v.3 constructed from high resolution DW-MRI data from 72 healthy subjects (26.6±4.8yr old, 30 males) (http://www.psy.cmu.edu/~coaxlab/data.html). Both datasets were pre-processed using conventional steps consisting of rigid body motion correction, correcting for nuisance variables (white matter, cerebrospinal fluid, motion parameters), and low pass filtering.

bioRxiv preprint doi: https://doi.org/10.1101/147611; this version posted June 8, 2017. The copyright holder for this preprint (which was not certified by peer review) is the author/funder, who has granted bioRxiv a license to display the preprint in perpetuity. It is made available under aCC-BY-NC-ND 4.0 International license.

The PD-ICA was used to assign a disease severity measure for each region at the first visit to determine a disease reservoir available for propagation[61].

Pearson correlation was used to investigate the relationship between disease progression in cortical areas (cortical thinning) and the 'disease exposure' for each region in the PD-ICA (defined by the average values of each region weighted by connectivity). The same procedure was performed to test propagation hypotheses along the functional and structural connectomes. The propagation analysis was performed for the whole brain and for each hemisphere separately.

CSF Measures

CSF $A\beta_{42}$, α-syn, t-tau, and p-tau_{181} from aliquots were assessed as previously described[62,63]. The MAP Luminex platform (Luminex Corp, Austin, TX) with Innogenetics (INNO-BIA AlzBio3; Ghent, Belgium; for research use-only reagents) immunoassays was used for $A\beta_{42}$, t-tau and p-tau_{181}. CSF α-syn assay was performed at Covance using a commercially available ELISA assay kit (Covance, Dedham, MA)[64]. To evaluate the possible contamination of blood in CSF – a factor thought to influence the level of some proteins including α-syn and $A\beta_{42}$[65,66] – the relationship between CSF hemoglobin and other CSF measures was assessed. No significant association was observed (all $p<0.05$), suggesting that there is no effect of added blood on concentration of CSF measures. Due to the ongoing nature of the study and incomplete data, only CSF data from baseline was used in this analysis[64].

bioRxiv preprint doi: https://doi.org/10.1101/147611; this version posted June 8, 2017. The copyright holder for this preprint (which was not certified by peer review) is the author/funder, who has granted bioRxiv a license to display the preprint in perpetuity. It is made available under aCC-BY-NC-ND 4.0 International license.

Acknowledgements

PPMI – a public-private partnership – is funded by the Michael J. Fox Foundation for Parkinson's Research and funding partners, including AbbVie, Avid, Biogen, Bristol-Myers Squibb, Covance, GE Healthcare, Genentech, GlaxoSmithKline, Lilly, Lundbeck, Merck, Meso Scale Discovery, Pfizer, Piramal, Roche, Sanofi Genzyme, Servier, Teva, and UCB.

Research supported by grants from the Michael J Fox Foundation for Parkinson's Research, the W. Garfield Weston Foundation, and the Alzheimer's Association, the Canadian Institutes of Health Research, and the Natural Sciences and Engineering Research Council of Canada to A. Dagher. Y. Yau is a Vanier Scholar and receives funding from the Canadian Institute of Health Research. Y. Zeighami holds the Jeanne Timmins Costello Fellowship. U. Vainik is supported by the Estonian Research Council (grant No. PUTJD6549).

Author Contributions

YY, YZ and AD contributed to the study design and interpretation. YY, YZ, TB, KL, UV, and MD analyzed the data. YY drafted the initial manuscript; all authors contributed to writing of this manuscript.

Competing Financial Interests

None.

bioRxiv preprint doi: https://doi.org/10.1101/147611; this version posted June 8, 2017. The copyright holder for this preprint (which was not certified by peer review) is the author/funder, who has granted bioRxiv a license to display the preprint in perpetuity. It is made available under aCC-BY-NC-ND 4.0 International license.

References

1 Seeley, W. W., Crawford, R. K., Zhou, J., Miller, B. L. & Greicius, M. D. Neurodegenerative diseases target large-scale human brain networks. *Neuron* **62**, 42-52, doi:10.1016/j.neuron.2009.03.024 (2009).

2 Warren, J. D. *et al.* Molecular nexopathies: a new paradigm of neurodegenerative disease. *Trends Neurosci* **36**, 561-569, doi:10.1016/j.tins.2013.06.007 (2013).

3 Burre, J. *et al.* Alpha-synuclein promotes SNARE-complex assembly in vivo and in vitro. *Science* **329**, 1663-1667, doi:10.1126/science.1195227 (2010).

4 Olanow, C. W. & Brundin, P. Parkinson's disease and alpha synuclein: is Parkinson's disease a prion-like disorder? *Movement disorders : official journal of the Movement Disorder Society* **28**, 31-40, doi:10.1002/mds.25373 (2013).

5 Luk, K. C. *et al.* Pathological alpha-synuclein transmission initiates Parkinson-like neurodegeneration in nontransgenic mice. *Science* **338**, 949-953, doi:10.1126/science.1227157 (2012).

6 Braak, H. *et al.* Staging of brain pathology related to sporadic Parkinson's disease. *Neurobiology of Aging* **24**, 197-211, doi:http://dx.doi.org/10.1016/S0197-4580(02)00065-9 (2003).

7 Marek, K. *et al.* The Parkinson Progression Marker Initiative (PPMI). *Progress in Neurobiology* **95**, 629-635, doi:http://dx.doi.org/10.1016/j.pneurobio.2011.09.005 (2011).

8 Zeighami, Y. *et al.* Network structure of brain atrophy in de novo Parkinson's disease. *eLife* **4**, e08440, doi:10.7554/eLife.08440 (2015).

9 Hely, M. A., Reid, W. G., Adena, M. A., Halliday, G. M. & Morris, J. G. The Sydney multicenter study of Parkinson's disease: the inevitability of dementia at 20 years.

bioRxiv preprint doi: https://doi.org/10.1101/147611; this version posted June 8, 2017. The copyright holder for this preprint (which was not certified by peer review) is the author/funder, who has granted bioRxiv a license to display the preprint in perpetuity. It is made available under aCC-BY-NC-ND 4.0 International license.

Movement disorders : official journal of the Movement Disorder Society **23**, 837-844, doi:10.1002/mds.21956 (2008).

10 Aarsland, D. *et al.* Cognitive decline in Parkinson disease. *Nature reviews. Neurology* **13**, 217-231, doi:10.1038/nrneurol.2017.27 (2017).

11 Dirnberger, G. & Jahanshahi, M. Executive dysfunction in Parkinson's disease: a review. *J Neuropsychol* **7**, 193-224, doi:10.1111/jnp.12028 (2013).

12 Callesen, M. B., Weintraub, D., Damholdt, M. F. & Moller, A. Impulsive and compulsive behaviors among Danish patients with Parkinson's disease: prevalence, depression, and personality. *Parkinsonism Relat Disord* **20**, 22-26, doi:10.1016/j.parkreldis.2013.09.006 (2014).

13 Ffytche, D. H. *et al.* The psychosis spectrum in Parkinson disease. *Nature reviews. Neurology* **13**, 81-95, doi:10.1038/nrneurol.2016.200 (2017).

14 Reetz, K. *et al.* Structural imaging in the presymptomatic stage of genetically determined parkinsonism. *Neurobiol Dis* **39**, 402-408, doi:10.1016/j.nbd.2010.05.006 (2010).

15 Fioravanti, V. *et al.* MRI Correlates of Parkinson's Disease Progression: A Voxel Based Morphometry Study. *Parkinson's Disease* **2015**, 8, doi:10.1155/2015/378032 (2015).

16 Camicioli, R. *et al.* Voxel-based morphometry reveals extra-nigral atrophy patterns associated with dopamine refractory cognitive and motor impairment in parkinsonism. *Parkinsonism & Related Disorders* **15**, 187-195, doi:http://dx.doi.org/10.1016/j.parkreldis.2008.05.002 (2009).

17 Menke, R. A. *et al.* Comprehensive morphometry of subcortical grey matter structures in early-stage Parkinson's disease. *Human brain mapping* **35**, 1681-1690 (2014).

bioRxiv preprint doi: https://doi.org/10.1101/147611; this version posted June 8, 2017. The copyright holder for this preprint (which was not certified by peer review) is the author/funder, who has granted bioRxiv a license to display the preprint in perpetuity. It is made available under aCC-BY-NC-ND 4.0 International license.

18 Davatzikos, C. Why voxel-based morphometric analysis should be used with great caution when characterizing group differences. *NeuroImage* **23**, 17-20, doi:http://dx.doi.org/10.1016/j.neuroimage.2004.05.010 (2004).

19 Hutton, C., Draganski, B., Ashburner, J. & Weiskopf, N. A comparison between voxel-based cortical thickness and voxel-based morphometry in normal aging. *Neuroimage* **48**, 371-380, doi:10.1016/j.neuroimage.2009.06.043 (2009).

20 Pereira, J. B. *et al.* Assessment of cortical degeneration in patients with Parkinson's disease by voxel-based morphometry, cortical folding, and cortical thickness. *Hum Brain Mapp* **33**, 2521-2534, doi:10.1002/hbm.21378 (2012).

21 Khundrakpam, B. S., Lewis, J. D., Kostopoulos, P., Carbonell, F. & Evans, A. C. Cortical Thickness Abnormalities in Autism Spectrum Disorders Through Late Childhood, Adolescence, and Adulthood: A Large-Scale MRI Study. *Cerebral Cortex* **27**, 1721-1731 (2017).

22 Dickerson, B. C. *et al.* The cortical signature of Alzheimer's disease: regionally specific cortical thinning relates to symptom severity in very mild to mild AD dementia and is detectable in asymptomatic amyloid-positive individuals. *Cerebral cortex (New York, N.Y. : 1991)* **19**, 497-510, doi:10.1093/cercor/bhn113 (2009).

23 Ibarretxe-Bilbao, N. *et al.* Progression of cortical thinning in early Parkinson's disease. *Movement disorders : official journal of the Movement Disorder Society* **27**, 1746-1753, doi:10.1002/mds.25240 (2012).

24 Jubault, T. *et al.* Patterns of cortical thickness and surface area in early Parkinson's disease. *Neuroimage* **55**, 462-467, doi:10.1016/j.neuroimage.2010.12.043 (2011).

bioRxiv preprint doi: https://doi.org/10.1101/147611; this version posted June 8, 2017. The copyright holder for this preprint (which was not certified by peer review) is the author/funder, who has granted bioRxiv a license to display the preprint in perpetuity. It is made available under aCC-BY-NC-ND 4.0 International license.

25 Zarei, M. *et al.* Cortical thinning is associated with disease stages and dementia in Parkinson's disease. *Journal of neurology, neurosurgery, and psychiatry* **84**, 875-882, doi:10.1136/jnnp-2012-304126 (2013).

26 Pereira, J. B. *et al.* Initial cognitive decline is associated with cortical thinning in early Parkinson disease. *Neurology* **82**, 2017-2025, doi:10.1212/wnl.0000000000000483 (2014).

27 Yeo, B. T. *et al.* The organization of the human cerebral cortex estimated by intrinsic functional connectivity. *Journal of neurophysiology* **106**, 1125-1165 (2011).

28 Cammoun, L. *et al.* Mapping the human connectome at multiple scales with diffusion spectrum MRI. *Journal of Neuroscience Methods* **203**, 386-397, doi:http://dx.doi.org/10.1016/j.jneumeth.2011.09.031 (2012).

29 Braak, H. & Braak, E. Pathoanatomy of Parkinson's disease. *Journal of Neurology* **247**, II3-II10, doi:10.1007/pl00007758 (2000).

30 Aarsland, D. & Kurz, M. W. The epidemiology of dementia associated with Parkinson disease. *Journal of the Neurological Sciences* **289**, 18-22, doi:http://dx.doi.org/10.1016/j.jns.2009.08.034 (2010).

31 Hwang, J. *et al.* Prediction of Alzheimer's disease pathophysiology based on cortical thickness patterns. *Alzheimer's & Dementia: Diagnosis, Assessment & Disease Monitoring* **2**, 58-67, doi:http://dx.doi.org/10.1016/j.dadm.2015.11.008 (2016).

32 Greicius, M. D., Srivastava, G., Reiss, A. L. & Menon, V. Default-mode network activity distinguishes Alzheimer's disease from healthy aging: evidence from functional MRI. *Proc Natl Acad Sci U S A* **101**, 4637-4642, doi:10.1073/pnas.0308627101 (2004).

bioRxiv preprint doi: https://doi.org/10.1101/147611; this version posted June 8, 2017. The copyright holder for this preprint (which was not certified by peer review) is the author/funder, who has granted bioRxiv a license to display the preprint in perpetuity. It is made available under aCC-BY-NC-ND 4.0 International license.

33 Koch, W. *et al.* Diagnostic power of default mode network resting state fMRI in the detection of Alzheimer's disease. *Neurobiology of Aging* **33**, 466-478, doi:http://dx.doi.org/10.1016/j.neurobiolaging.2010.04.013 (2012).

34 Sheline, Y. I. *et al.* Amyloid Plaques Disrupt Resting State Default Mode Network Connectivity in Cognitively Normal Elderly. *Biological psychiatry* **67**, 584-587, doi:http://dx.doi.org/10.1016/j.biopsych.2009.08.024 (2010).

35 Braak, H. & Braak, E. Frequency of Stages of Alzheimer-Related Lesions in Different Age Categories. *Neurobiology of Aging* **18**, 351-357, doi:http://doi.org/10.1016/S0197-4580(97)00056-0 (1997).

36 Villain, N. *et al.* Regional dynamics of amyloid-β deposition in healthy elderly, mild cognitive impairment and Alzheimer's disease: a voxelwise PiB–PET longitudinal study. *Brain* **135**, 2126-2139, doi:10.1093/brain/aws125 (2012).

37 Palmqvist, S. *et al.* Accuracy of brain amyloid detection in clinical practice using cerebrospinal fluid beta-amyloid 42: a cross-validation study against amyloid positron emission tomography. *JAMA Neurol* **71**, 1282-1289, doi:10.1001/jamaneurol.2014.1358 (2014).

38 Gomperts, S. N. *et al.* PET Radioligands Reveal the Basis of Dementia in Parkinson's Disease and Dementia with Lewy Bodies. *Neuro-degenerative diseases* **16**, 118-124, doi:10.1159/000441421 (2016).

39 Alves, G. *et al.* CSF Aβ42 predicts early-onset dementia in Parkinson disease. *Neurology* **82**, 1784-1790, doi:10.1212/WNL.0000000000000425 (2014).

40 Irwin, D. J. *et al.* Neuropathologic substrates of Parkinson disease dementia. *Annals of neurology* **72**, 587-598, doi:10.1002/ana.23659 (2012).

bioRxiv preprint doi: https://doi.org/10.1101/147611; this version posted June 8, 2017. The copyright holder for this preprint (which was not certified by peer review) is the author/funder, who has granted bioRxiv a license to display the preprint in perpetuity. It is made available under aCC-BY-NC-ND 4.0 International license.

41 Frey, K. A. & Petrou, M. Imaging Amyloidopathy in Parkinson Disease and Parkinsonian Dementia Syndromes. *Clinical and translational imaging* **3**, 57-64, doi:10.1007/s40336-015-0104-4 (2015).

42 Sepulcre, J. *et al.* In vivo tau, amyloid, and gray matter profiles in the aging brain. *Journal of Neuroscience* **36**, 7364-7374 (2016).

43 Thomas, C. *et al.* Anatomical accuracy of brain connections derived from diffusion MRI tractography is inherently limited. *Proc Natl Acad Sci U S A* **111**, 16574-16579, doi:10.1073/pnas.1405672111 (2014).

44 Jones, D. K., Knosche, T. R. & Turner, R. White matter integrity, fiber count, and other fallacies: the do's and don'ts of diffusion MRI. *Neuroimage* **73**, 239-254, doi:10.1016/j.neuroimage.2012.06.081 (2013).

45 Raj, A., Kuceyeski, A. & Weiner, M. A network diffusion model of disease progression in dementia. *Neuron* **73**, 1204-1215, doi:10.1016/j.neuron.2011.12.040 (2012).

46 Iturria-Medina, Y., Sotero, R. C., Toussaint, P. J., Evans, A. C. & and the Alzheimer's Disease Neuroimaging, I. Epidemic Spreading Model to Characterize Misfolded Proteins Propagation in Aging and Associated Neurodegenerative Disorders. *PLOS Computational Biology* **10**, e1003956, doi:10.1371/journal.pcbi.1003956 (2014).

47 Yarkoni, T., Poldrack, R. A., Nichols, T. E., Van Essen, D. C. & Wager, T. D. Large-scale automated synthesis of human functional neuroimaging data. *Nature methods* **8**, 665-670 (2011).

48 Chklovskii, D. B., Mel, B. & Svoboda, K. Cortical rewiring and information storage. *Nature* **431**, 782-788 (2004).

bioRxiv preprint doi: https://doi.org/10.1101/147611; this version posted June 8, 2017. The copyright holder for this preprint (which was not certified by peer review) is the author/funder, who has granted bioRxiv a license to display the preprint in perpetuity. It is made available under aCC-BY-NC-ND 4.0 International license.

49 la Fougère, C. *et al.* Where in-vivo imaging meets cytoarchitectonics: The relationship between cortical thickness and neuronal density measured with high-resolution [18F]flumazenil-PET. *NeuroImage* **56**, 951-960, doi:http://dx.doi.org/10.1016/j.neuroimage.2010.11.015 (2011).

50 Ad-Dab'bagh, Y. *et al.* in *Proceedings of the 12th annual meeting of the Organization for Human Brain Mapping.* 2266.

51 Fonov, V. S., Evans, A. C., McKinstry, R. C., Almli, C. & Collins, D. Unbiased nonlinear average age-appropriate brain templates from birth to adulthood. *NeuroImage* **47**, S102 (2009).

52 Fonov, V. *et al.* Unbiased average age-appropriate atlases for pediatric studies. *NeuroImage* **54**, 313-327, doi:http://dx.doi.org/10.1016/j.neuroimage.2010.07.033 (2011).

53 Sled, J. G., Zijdenbos, A. P. & Evans, A. C. A nonparametric method for automatic correction of intensity nonuniformity in MRI data. *IEEE transactions on medical imaging* **17**, 87-97, doi:10.1109/42.668698 (1998).

54 Simmons, A. *et al.* The AddNeuroMed framework for multi-centre MRI assessment of Alzheimer's disease: experience from the first 24 months. *International journal of geriatric psychiatry* **26**, 75-82 (2011).

55 Kim, J. S. *et al.* Automated 3-D extraction and evaluation of the inner and outer cortical surfaces using a Laplacian map and partial volume effect classification. *Neuroimage* **27**, 210-221, doi:10.1016/j.neuroimage.2005.03.036 (2005).

56 Worsley, K. J. *et al.* A unified statistical approach for determining significant signals in images of cerebral activation. *Human brain mapping* **4**, 58-73 (1996).

bioRxiv preprint doi: https://doi.org/10.1101/147611; this version posted June 8, 2017. The copyright holder for this preprint (which was not certified by peer review) is the author/funder, who has granted bioRxiv a license to display the preprint in perpetuity. It is made available under aCC-BY-NC-ND 4.0 International license.

57 Epskamp, S. semPlot: Unified visualizations of structural equation models. *Structural Equation Modeling: A Multidisciplinary Journal* **22**, 474-483 (2015).

58 Rosseel, Y. lavaan: An R Package for Structural Equation Modeling. *Journal of Statistical Software* **48**, 1-36 (2012).

59 R Core Team. *R: A language and environment for statistical computing.*, <https://www.R-project.org/> (2015).

60 Coupé, P. *et al.* An optimized blockwise nonlocal means denoising filter for 3-D magnetic resonance images. *IEEE transactions on medical imaging* **27**, 425-441 (2008).

61 Mišić, B. *et al.* Cooperative and Competitive Spreading Dynamics on the Human Connectome. *Neuron* **86**, 1518-1529, doi:10.1016/j.neuron.2015.05.035 (2015).

62 Kang, J., Irwin, D. J., Chen-Plotkin, A. S. & et al. Association of cerebrospinal fluid β-amyloid 1-42, t-tau, p-tau181, and α-synuclein levels with clinical features of drug-naive patients with early parkinson disease. *JAMA Neurology* **70**, 1277-1287, doi:10.1001/jamaneurol.2013.3861 (2013).

63 Toledo, J. B. *et al.* α-Synuclein improves diagnostic and prognostic performance of tau and Aβ in Alzheimer's disease. *Acta neuropathologica* **126**, 10.1007/s00401-00013-01148-z, doi:10.1007/s00401-013-1148-z (2013).

64 Mollenhauer, B. *et al.* Total CSF alpha-synuclein is lower in de novo Parkinson patients than in healthy subjects. *Neurosci Lett* **532**, 44-48, doi:10.1016/j.neulet.2012.11.004 (2013).

65 Bjerke, M. *et al.* Confounding Factors Influencing Amyloid Beta Concentration in Cerebrospinal Fluid. *International Journal of Alzheimer's Disease* **2010**, 986310, doi:10.4061/2010/986310 (2010).

bioRxiv preprint doi: https://doi.org/10.1101/147611; this version posted June 8, 2017. The copyright holder for this preprint (which was not certified by peer review) is the author/funder, who has granted bioRxiv a license to display the preprint in perpetuity. It is made available under aCC-BY-NC-ND 4.0 International license.

66 Hong, Z. *et al.* DJ-1 and α-synuclein in human cerebrospinal fluid as biomarkers of Parkinson's disease. *Brain* **133**, 713-726 (2010).